

## A new multifunctional converter based on a series compensator applied to AC microgrids

Hélio Marcos André Antunes\*, Sidelmo Magalhães Silva, Danilo Iglesias Brandao, Alysson Augusto Pereira Machado, Braz de Jesus Cardoso Filho

Graduate Program in Electrical Engineering, Federal University of Minas Gerais, Av. Antônio Carlos 6627, 31270-901 Belo Horizonte, Minas Gerais, Brazil



### ARTICLE INFO

**Keywords:**

AC microgrids  
Distributed generation  
Multifunctional converter  
Power quality  
Hardware-in-the-loop simulation

### ABSTRACT

This paper proposes a new multifunctional converter based on a series voltage compensator applied to centralized AC microgrids. Besides the basic functionalities required for a centralized converter in microgrids, such as grid-supporting and grid-forming voltage support and smooth transition from operating modes, the proposed converter can change its connection topology from series to parallel and vice-versa, depending on the system's condition. Thus, it assumes all the basic defining features of series and shunt power converters. The devised control algorithm allows on-line change of converter operating modes either as voltage- or current-controlled sources. These flexible functionalities allow the converter to operate as: (i) a grid-forming converter providing voltage and frequency references for the entire microgrid, keeping the voltages at the point of common coupling (PCC) synchronized with the utility voltage; (ii) grid-feeding active power into the microgrid; and (iii) grid-supporting, performing ancillary services such as voltage regulation, voltage sag and swell compensation, along with active power filtering, reactive power, unbalance and harmonic compensation. The converter can be applied to both single-phase and three-phase three- or four-wire networks. The multifunctional control is implemented using a Texas Instruments TMS320F28335 digital signal processor, and then validated through a hardware-in-the-loop simulation developed in the Typhoon HIL 600 platform.

### 1. Introduction

Nowadays, electrical power systems are moving toward endowing consumers with small generators, called distributed generators (DGs), which drastically change basic power systems defining characteristics from unidirectional to bi-directional power flow. The main arguments for this change are of an economical, technical and political nature [1]. This change occurs mainly due to advances in power electronics technology and high penetration of renewable energy sources, such as wind and photovoltaic (PV) [2,3]. In this context, the concept of a microgrid emerges as a decentralized model to structure modern power systems. A microgrid is defined as a set of DGs, loads and energy storage elements gathered and controlled as a single dispatchable unit able to operate either in grid-connected or in islanded mode [4–6].

Power converters used in microgrids are usually based on the voltage source inverters (VSIs) and they can be divided into three categories, depending on their operating duties and functions [7–9]. The first category is the grid-feeding converter that operates injecting active power into the grid and is usually controlled as a current source in P-Q (active-reactive power) mode. The second is the grid-forming converter

that supplies loads as a voltage source and often operates in V-f (voltage-frequency) mode [4,10]. Finally, the grid-supporting converter performs ancillary services such as voltage and frequency regulation, harmonic filtering and low voltage ride-through. This latter may be controlled either as a voltage or current source [11].

Multifunctional converters have attracted attention to micro-grid applications, as it is possible to use the existing DG power interface, performing ancillary services and improving the power efficiency and quality of the power system [12,13]. In [14] a PV power system equipped with a battery bank operating as a hybrid inverter is shown, which means that this DG can act as both a grid-feeding converter or a grid-forming converter.

In centralized microgrids with master-slave architecture, a centralized converter, also called grid-interactive interface, provides grid-forming and grid-supporting functionalities. This sort of converter is often connected in parallel with the microgrid [11,15,16]. In [16] during grid-connected mode, the converter directly controls the injected current and may compensate reactive power, unbalance and harmonics. On the other hand, in an islanded mode, the converter is responsible for providing voltage and frequency references for the

\* Corresponding author.

E-mail address: [helioantunes@ufmg.br](mailto:helioantunes@ufmg.br) (H.M.A. Antunes).

microgrid. Another crucial feature of this converter is the ability to handle seamless transition from grid-connected to islanded mode and vice-versa. In [17], a generalized control algorithm that allows a three-phase inverter to perform the essential functions of microgrid's converters, with seamless transition between modes of operation, is described. The shunt converter has bi-directional capacity and may operate as voltage- or current-controlled source in a decentralized AC microgrid. In a grid-connected mode, it can concurrently inject active power and regulate reactive power to perform voltage support. While during islanded operation, voltage and frequency are controlled based on droop characteristics.

In addition, there are also grid-interactive converters based on series voltage compensators [18]. During grid-connected mode, this converter operates as a series active power filter compensating voltage disturbances, such as harmonics, sag and swell on the grid voltage, and as an isolating device (i.e., isolating downstream faults in a microgrid). In an islanded mode, it runs as an on-line uninterruptible power supply (UPS). It may also provide smooth transition from grid-connected to islanded mode and vice-versa.

This paper proposes a multifunctional converter based on a series voltage compensator capable of operating either in parallel or in series connection, depending on both grid and microgrid conditions. Therefore, it performs all the basic functions of series and parallel power converters, without requiring two converters, as in a back-to-back topology. The devised control algorithm also allows the converter to seamlessly change its operation either as a voltage- or current-controlled source. The multifunctionalities of the proposed converter with specific functions are: (i) grid-forming converter providing voltage and frequency references, smooth transition from grid-connected to islanded mode and vice-versa; (ii) grid-feeding converter injecting active power into the grid; and finally (iii) grid-supporting converter, acting as a series and shunt active power filter, regulating voltage, compensating voltage sags and swells, and enhancing the power factor (i.e., reactive, unbalance and harmonic compensation).

The main contribution of this paper is the flexible multifunctional converter that can operate in series or parallel with the microgrid exploiting both connection topology. Such a converter can operate performing the basic functions of the well-known microgrid converters, with the proper transition between operating modes. To the best of the authors' knowledge, no centralized multifunctional converter for AC microgrid application endowed with both defining features of series and shunt converters was presented in the literature previously.

## 2. Proposed multifunctional converter

The proposed multifunctional converter is based on a series voltage compensator with converter structure presented in [19]. Furthermore, by making some changes in the control algorithm and output filter, it is feasibly adapted to operate as a voltage- or current-controlled source, depending on the system needs. Fig. 1 shows the single-phase diagram of the proposed converter applied to an AC microgrid. The voltage source at the DC side of VSI represents a battery bank and a buck-boost converter to enable bidirectional power flow, comprising an energy storage system (ESS) [20].

Besides the conventional topology of series compensator, it has included a non-time-critical switch breaker ( $S_1$ ) and two static switches (SS-MG and SS-G) as shown in Fig. 1. Switch SS-BP is usually presented in conventional series voltage compensator topologies [21]. The additional switches  $S_1$ , SS-G and SS-BP allow the converter to be connected either in series or in parallel to the grid. The switch  $S_{\text{grid}}$  is not part of the converter and represents the utility operated breaker at the point of connection. The multifunctional converter is composed of single-phase H-bridge VSIs that can be applied to both single-phase and three-phase three- or four-wire networks.

The proposed converter can operate in five different modes, depending on the configuration of switches according to Table 1. State "0"

indicates an opened switch, while state "1" means the switch is closed. The steady state operating modes of the multifunctional converter are depicted in Fig. 2. The main modes of operation are:

- Mode I: The microgrid is disabled as shown in Fig. 2(a), e.g., microgrid under maintenance.
- Mode II: The multifunctional converter is inactive, but the point of common coupling (PCC) of the microgrid is supplied by the power grid, as shown in Fig. 2(b). This mode is required for converter maintenance or failure.
- Mode III: The converter is connected in series to the grid, operating as a grid-supporting converter, as shown in Fig. 2(c). In this mode, the converter may perform ancillary services, typical of series devices, compensating electric disturbances in the voltage waveform.
- Mode IV: The multifunctional converter is connected in shunt with the power grid, as shown in Fig. 2(d). Switches SS-MG, SS-BP and SS-G are closed as shown in Table 1. In this mode, the converter injects active power from the ESS, and it can perform typical ancillary services of shunt devices, compensating electric disturbances in the current waveform or regulating voltage through reactive power injection.
- Mode V: The converter operates in islanded mode working as a grid-forming converter, as shown in Fig. 2(e).

Fig. 3 shows the possible transitions between the converter operating modes. In transition  $T_1$ , the microgrid is turned on and the multifunctional converter operates in standby mode. In transition  $T_{II}$ , the converter is connected in series, while  $T_{III}$  sets the converter in shunt. Transitions  $I_{T-I}$  and  $I_{T-II}$  disconnect the multifunctional converter and microgrid from the main grid changing its switches and control scheme. The proper instant to open switches (SS-MG and  $S_1$ ) in  $I_{T-I}$  is during grid current zero crossing, which guarantees that switch SS-MG opens and SS-G closes without a short-circuit. In this paper, only the intentional islanding is evaluated.

Transitions  $R_{T-I}$  and  $R_{T-II}$  reconnect the microgrid to the mains. Initially, the converter voltage is synchronized with the grid. After, switches SS-MG and SS-BP are closed and the converter is connected in parallel ( $R_{T-I}$ ). It is also possible to reconnect the microgrid with the multifunctional converter in series ( $R_{T-II}$ ), keeping SS-MG and  $S_1$  closed. Additionally, the multifunctional converter can operate as a grid-forming converter, allowing a black-start ( $BS_T$ ) operation. Initially, the system is disabled as in mode I, then the multifunctional converter is turned on, and the PCC is energized in mode V. If necessary, the microgrid is reconnected to the grid and the converter operation can be changed to modes III or IV.

## 3. Design and control of the proposed multifunctional converter

A critical point for the multifunctional converter is the selection of the inverter topology and its output filter that allows both connection topologies (i.e., series or parallel), and operation modes (i.e., voltage- and current-controlled source) depending on the microgrid requirements. Thus, herein a transformerless single-phase VSI using an H-bridge topology associated with an ESS has been chosen [13]. In addition, the converter control needs to provide smooth transition between the operating modes, without interrupting the microgrid's loads.

### 3.1. Design of the LC output filter

The output filter of VSIs is used to reduce PWM switching ripple coupling between the grid and converter [22]. Herein, the design of the LC filter is based on the hybrid operation of the multifunctional converter, i.e., as a current- or voltage-controlled source. The capacitance of the LC filter is chosen to be equal to 7.5% of the converter rated power as in (1). A maximum current ripple of 30% is considered to calculate the inductance, using a three-level PWM as in (2) [23].

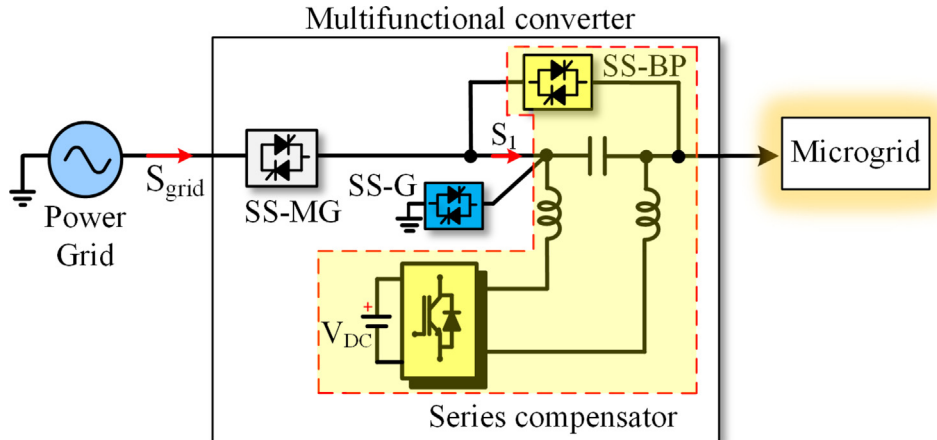


Fig. 1. Proposed single-phase multifunctional converter.

**Table 1**  
Switch configuration for the operating modes of the multifunctional converter.

| Mode | SS-MG | SS-BP | SS-G | S <sub>1</sub> |
|------|-------|-------|------|----------------|
| I    | 0     | 0     | 0    | 0              |
| II   | 1     | 1     | 0    | 0              |
| III  | 1     | 0     | 0    | 1              |
| IV   | 1     | 1     | 1    | 0              |
| V    | 0     | 0     | 1    | 0              |

Finally, calculate the cutoff frequency of the LC filter as a function of its parameters can be calculated defined in (3), using the separation of one decade between the converter switching frequency, i.e.,  $f_{sw} = 12\text{ kHz}$  [19].

$$C = \frac{KS_n}{2\pi f_f^2} \quad (1)$$

$$L = \frac{V_{DC}}{6f_{sw}\Delta_{iL}} \quad (2)$$

$$f_c = \frac{1}{2\pi\sqrt{LC}} \quad (3)$$

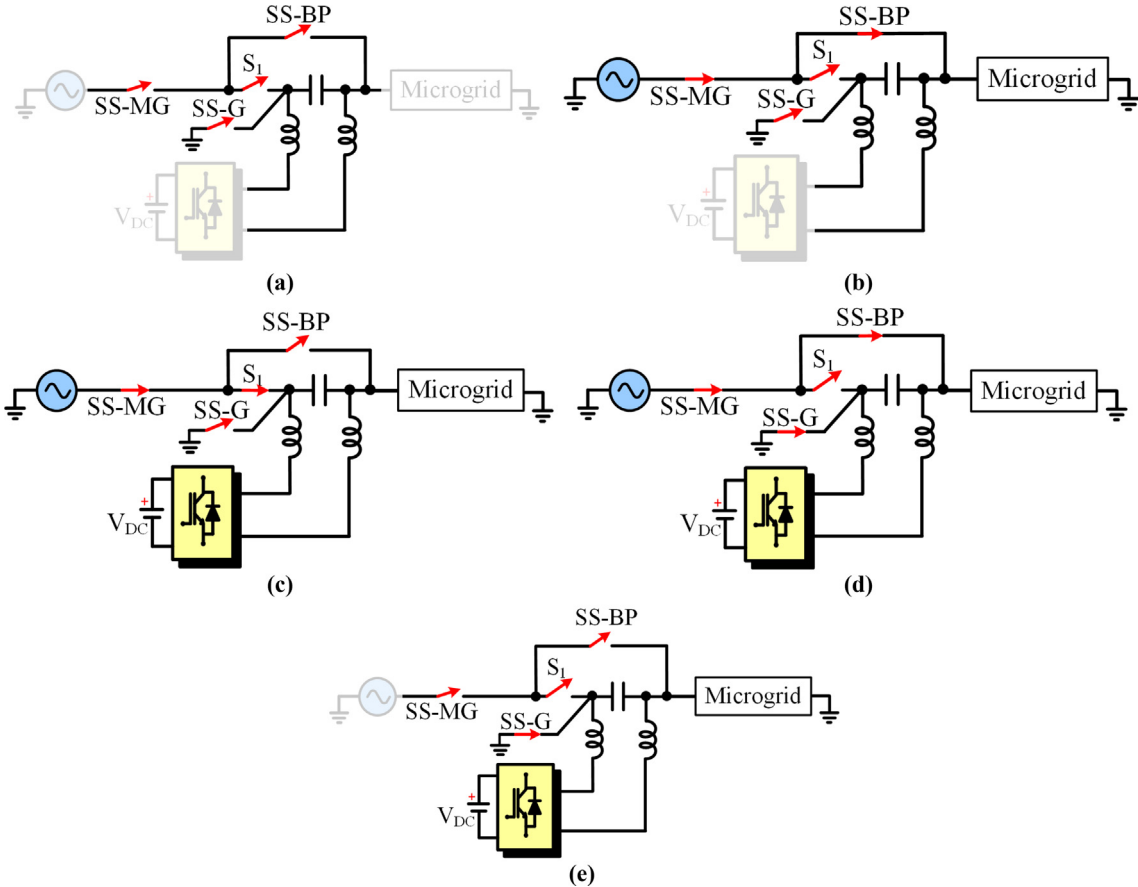


Fig. 2. Operating modes of the proposed converter: (a) mode I; (b) mode II; (c) mode III; (d) mode IV; (e) mode V.

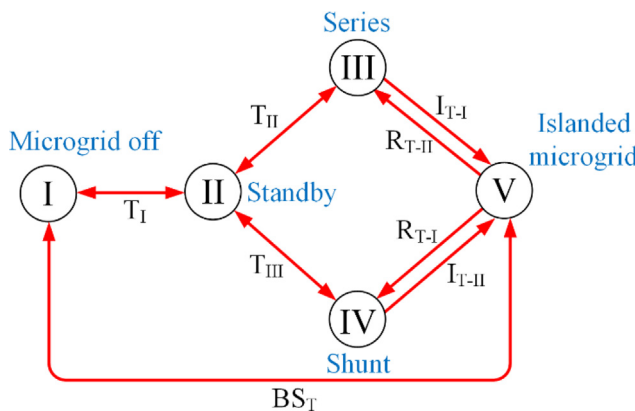


Fig. 3. Possible transitions between the operating modes.

- $S_n$  - nominal power [VA];      •  $\Delta_{IL}$  - maximum ripple of current [A];
- $V_f$  - output voltage [V];      •  $f_{sw}$  - switching frequency [Hz];
- $f$  - fundamental frequency [Hz];      •  $V_{DC}$  - DC link voltage [V].
- $K$  - adopted percentage

### 3.2. Converter control

Fig. 4(a) shows a single-phase diagram with all electric quantities required by the converter control. Fig. 4(b) shows the full control structure devised in natural (*abc*-frame) coordinates, using per unit (pu) values. Setting the value of flags “VS” and “CS” in Fig. 4(b), the converter control operates as current- or voltage-controlled source, as shown in Fig. 4(c) and (d), respectively.

#### 3.2.1. Current control

The current control mode is set through variables “VS = 0” and “CS = 1” in the control schematic of Fig. 4(b), disabling the voltage loop. Fig. 4(c) shows the current loop that comprises a parallel association between a plug-in RC (repetitive controller) for odd harmonics, and PI (proportional-integral) controller. The PI controller enhances the transient response, since the RC needs a minimum of half a cycle of the fundamental frequency to settle [24,25]. To improve the dynamic response of the current control mode, output grid voltage ( $v_{g,poll}$ ) and  $\hat{R}i_L$  are feedforward.

To design the gains of the PI controller, the RC and active damping ( $R_{p,i,c}$ ) are firstly disregarded. The current loop is designed considering the desired crossover frequency and phase margin of the open-loop transfer function obtained from Fig. 4(c) [26]. It is considered a crossover frequency of 900 Hz and a phase margin of 85°. This design method leads to  $K_{pi} = 0.44 \Omega$  and  $K_{ii} = 223 \Omega/\text{s}$ , using a current sensor ( $H_i$ ) gain equal to 1/280 ( $\text{VA}^{-1}$ ).

The stable operation of RC requires a low-pass filter (LPF) in its path, to adequate the control dynamics with the bandwidth of the power converter [25]. The LPF chosen is a second order structure defined in [27], with a cutoff frequency ( $w_c$ ) equal to 900 Hz. Using a digital implementation for the RC with  $T_s = 12 \text{ kHz}$ , a phase advance equal to three samples is added to compensate the displacement of poles caused by the LPF and PI, forcing the overall delay of the RC to be  $z^{(-100+2)}$ , with a gain  $K_r$  equal to 0.1.

#### 3.2.2. Voltage control

Fig. 4(d) shows the voltage control diagram that is obtained setting variables “VS = 1” and “CS = 0” in Fig. 4(b). Fig. 4(d) shows the control diagram, which comprises a parallel association between a

plug-in RC and a PI controller in cascade with a proportional controller in the current loop. Feedforward actions, including output voltage ( $v_o$ ), current ( $i_o$ ) and  $\hat{R}i_L$  are used to improve the system dynamic response [24,28,29].

For the inner current control, a crossover frequency of 1.2 kHz and a phase margin of 85° are chosen, while for the outer voltage loop, a bandwidth of 660 Hz and a phase margin of 60° are set [30]. The obtained gains are  $K_{pi} = 0.6 \Omega$ ,  $K_{pv} = 0.8 \Omega^{-1}$ , and  $K_{iv} = 68 \Omega^{-1}\text{s}^{-1}$ , adopting a voltage sensor ( $H_v$ ) gain equal to 1/150 ( $\text{VV}^{-1}$ ). For the RC used in the voltage loop, a LPF equal to the one used in the current loop was also applied, with a cutoff frequency equal to 900 Hz, and gain  $K_r$  set to 0.25.

#### 3.2.3. Voltage and current reference

**3.2.3.1. Voltage reference generator.** Fig. 5 shows the voltage reference block defined in Fig. 4(d), which allows the multifunctional converter to operate as a voltage-controlled source. A PLL based on the instantaneous inner product of orthogonal functions, as defined in [31], is used for the single-phase converters.

From Fig. 5, when flag  $ref\_v$  is zero, no voltage reference is generated. Whereas, when it is equal to one, the converter operates in mode III, i.e., providing series active filtering functionality. Initially, the PLL is synchronized with the grid setting flag  $sinc\_pll$  equal to one and generating a 60 Hz voltage reference ( $v_{g,poll}$ ). This reference signal is compared to the measured instantaneous grid voltage ( $v_g$ ) resulting in the voltage reference ( $v_{ref} = H_v v_{SAF}$ ).

To perform transition  $I_{T-I}$ , i.e., series connection to islanded mode, the procedure starts when flag  $ref\_v$  is switched to position number two in Fig. 5. Thus, the islanding detection algorithm sets flag  $sinc\_pll$  to zero. The feedforward action ( $w_o$ ) of the PLL leads to a sinusoidal waveform signal of 60 Hz, which can be multiplied by a unitary negative gain, forming the signal reference ( $v_T$ ). Thus, the converter operates in mode V as a grid-forming converter.

Considering the black-start procedure in Mode V, the voltage reference is generated setting flag  $ref\_v$  to position number 3 in Fig. 5. In this condition, the PLL ( $sinc\_pll$  equals zero) generates the sinusoidal voltage reference. However, the signal reference ( $v_{BS}$ ) is only activated with the flag  $ramp\_v$  set to one, which creates a voltage ramp within four cycles of the fundamental frequency.

Finally, the reconnection transition ( $R_{T-II}$ ) from islanded (i.e., mode V) to series grid-connected operation (i.e., mode III) is performed switching flag  $ref\_v$  to position number one. However, it can just be done, if and only if flag  $sinc\_pll$  is equal to one, indicating that the microgrid voltage is synchronized with the grid voltage to comply with the grid codes.

**3.2.3.2. Current reference generator.** The current reference block, shown in Fig. 4(c), is detailed in Fig. 6. This control strategy allows the multifunctional converter to operate as a current-controlled source. When  $flag\_i$  is zero, no current reference is generated.

To perform the transition  $R_{T-I}$ , i.e., islanded to shunt grid-connected mode, the converter is initially operated as a voltage-controlled source, with flag  $ref\_v$  equal to 3, and flag  $sinc\_pll$  equal to 1, ensuring the voltage synchronization as in Fig. 5. Then  $flag\_i$  can be changed to position 1 in Fig. 6 driving the converter to mode IV, operating as a current-controlled source (i.e., shunt grid-connected operation). Concurrently, flag  $ref\_v$  goes automatically to zero. To avoid overvoltage at the microgrid’s PCC during transition, the multifunctional converter instantly supplies the full microgrid demand ( $i_{MG}$ ) and the LC filter capacitive current ( $i_{cap,LC}$ ), increasing the exchanged power with the grid in a ramp within four cycles of fundamental frequency. If the converter needs to move to mode II (i.e., standby), it is firstly required to cease the injection of power and then switch  $flag\_i$  to zero. It is also possible to operate in mode IV, with  $flag\_i$  equal to 2 or 3.

To control the multifunctional converter under PQ mode,  $flag\_i$  is set

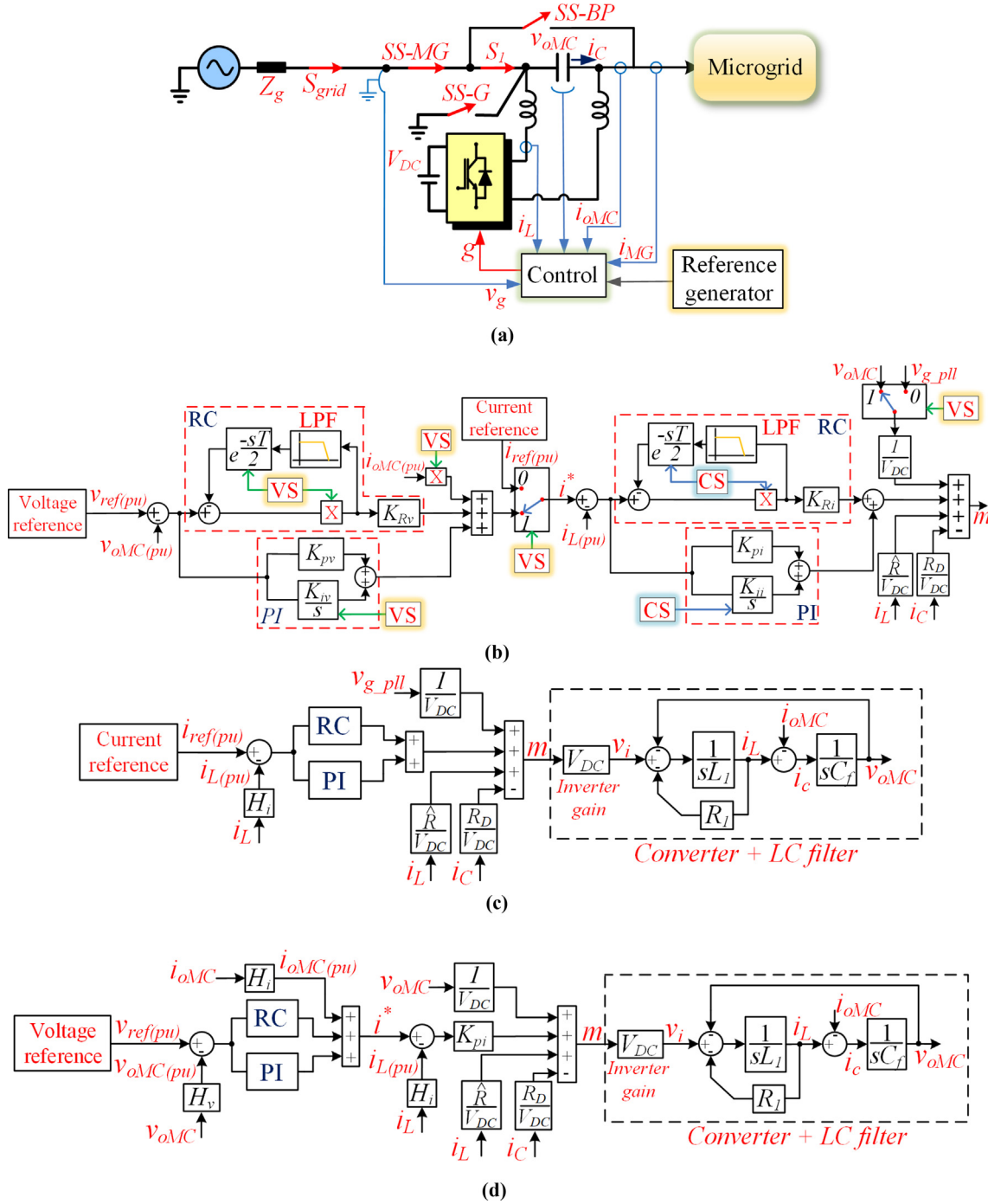


**Fig. 4.** Control of the multifunctional converter: (a) diagram of connection and sensors; (b) full control scheme; (c) current-controlled source; (d) voltage-controlled source.

to position number 2 in Fig. 6. In this condition, the PLL ensures grid voltage synchronization ( $v_{g,poll}$ ), while signals  $v_{g,\cos\theta}$  and  $v_{g,\sin\theta}$  shape the instantaneous current references. The PQ control loops, responsible for generating the current references for active and reactive power injection, are based on PI controllers with the following gains:  $K_p = 0.1 \text{ A}^{-1}$  and  $K_i = 200 \text{ A}^{-1}\text{s}^{-1}$  [32].

Finally, setting flag  $i$  to position 3, the shunt active filtering functionality is selected. The current reference is generated based on the conservative power theory (CPT) [33]. In addition, reactive power is injected to supply the capacitive current of the LC filter.

### 3.2.4. Active damping of the LC filter

A challenging issue in the application of VSI with an LC output filter is the resonance peak in its frequency response. Possible solutions to attenuate the resonance peak are based on active or passive techniques [22]. Passive techniques use resistors in parallel or series with capacitor or inductor of the filter, whereas, active damping techniques produce a virtual resistance in the LC filter, using some modification in the converter control [34,35].

For the proposed multifunctional converter an active damping technique using the capacitor current was adopted. Fig. 7 shows two different operating modes of the proposed converter, where the closed switches are not shown. Fig. 7(a) shows the multifunctional converter

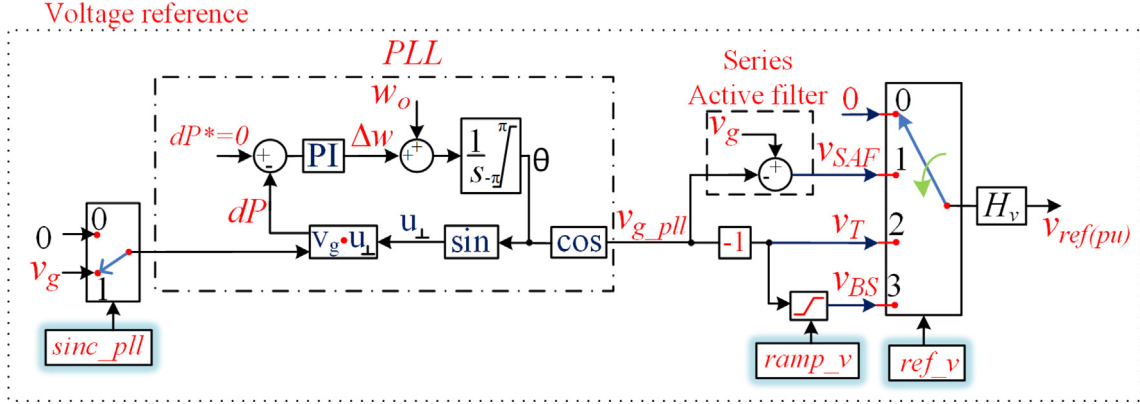


Fig. 5. Voltage reference block for the multifunctional converter.

in islanded mode V as a grid-forming converter. In Fig. 7(b), the converter is shunt connected to the power grid, operating as a current source in mode IV. For both cases, a damping term ( $R_{Df}$ ) is added to the converter control scheme, as illustrated in Fig. 7(c) and (d). The term ( $R_{Df}$ ) emulates a voltage-controlled source at the output of the converter, as shown in Fig. 7(a) and (b), and provides the required damping to the LC filter.

The transfer function of the stand-alone converter with the LC output filter supplying a passive load, including the active damping strategy is presented in (4). For the case that the converter is connected to the grid through a LC filter, Eq. (5) presents its transfer function  $i_L(s)/v_i(s)$ .

$$\frac{v_{oMC}(s)}{v_i(s)} = \frac{1}{s^2 L_1 C_f + s C_f (R_i + R_D) + 1} \quad (4)$$

$$\frac{i_L(s)}{v_i(s)} = \frac{s^2 L_g C_f + s C_f R_g + 1}{s^3 L_1 L_g C_f + s^2 (L_1 R_g C_f + R_l L_g C_f + R_D L_g C_f) + s (R_g C_f R_D + C_f R_g R_l + L_1 + L_g) + (R_l + R_D + R_g)} \quad (5)$$

Fig. 8 shows the frequency response of both transfer functions. As can be seen in Fig. 8(a), increasing the  $R_D$  value leads to higher attenuation of the resonance peak of the system in isolated operation. An essential feature of this technique is the fact that in frequencies above the attenuation frequency, the filter maintains an attenuation of 40 dB/dec. Considering the grid-connected mode, the increasing of the  $R_D$  value also allows the reduction of the harmonic amplification between the LC filter and the grid, as shown in Fig. 8(b). A  $R_D$  value equal to  $0.25 \Omega$  is used in the multifunctional control.

#### 4. Hardware-in-the-loop results

Hardware-in-the-loop simulations based on Typhoon HIL 600 were used to evaluate the control of the proposed multifunctional converter,

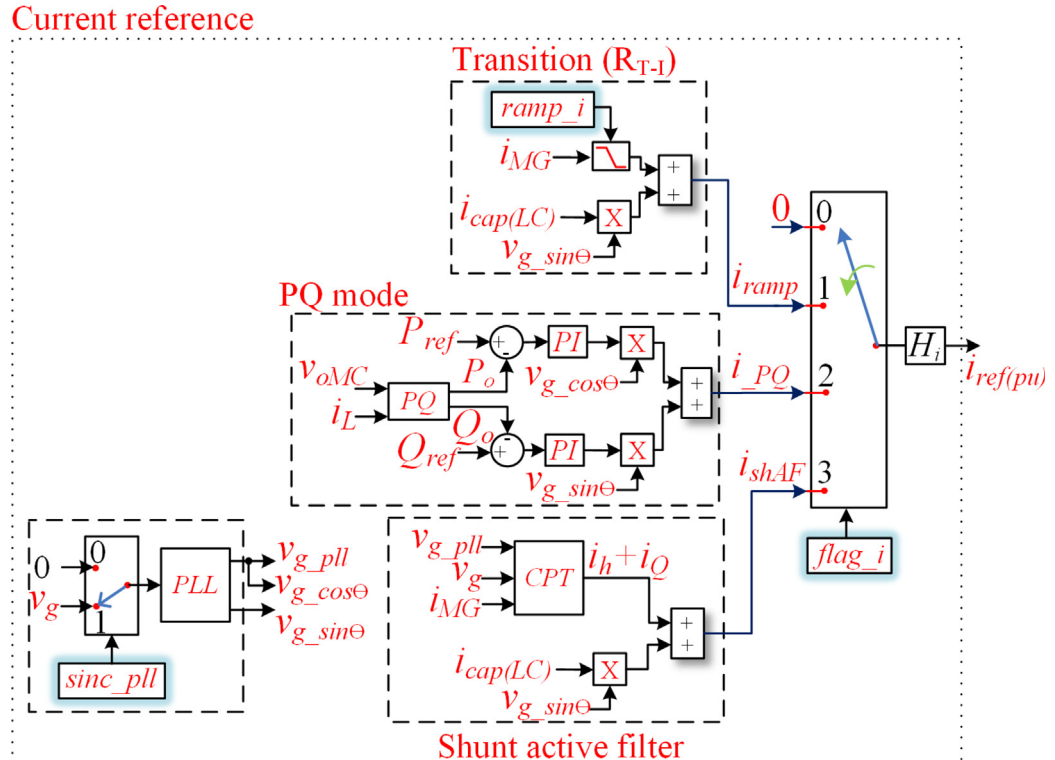
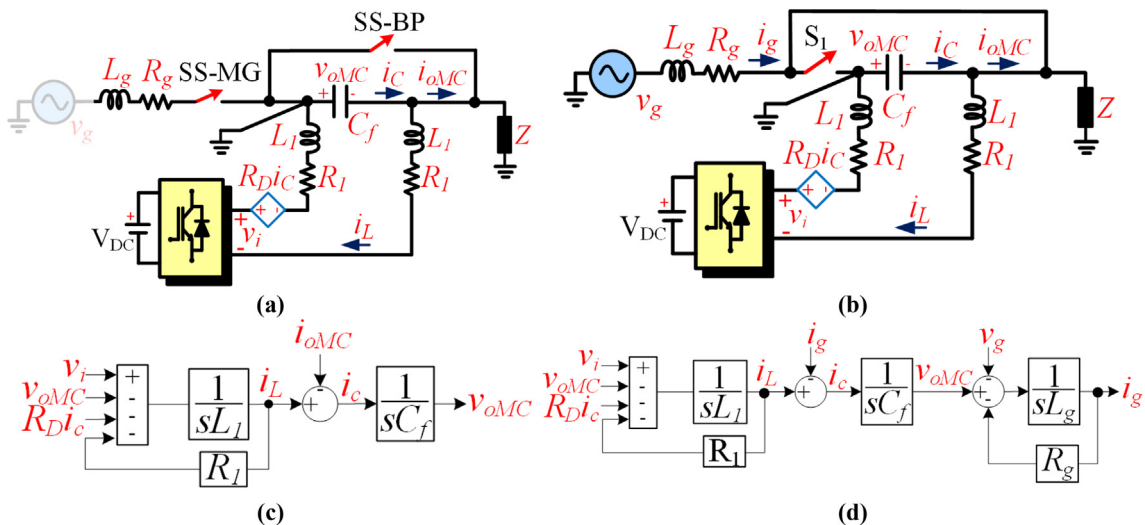


Fig. 6. Current reference block for the multifunctional converter.



**Fig. 7.** Single line diagram of multifunctional converter: (a) islanded mode (mode V); (b) grid-connected mode (mode IV); (c) block diagram of the LC filter in islanded; and (d) grid-connected mode.

as shown in Fig. 9. Table 2 summarizes the main electrical parameters of the microgrid under analysis.

Two Texas digital signal processors (TMS320F28335) are used. One processor is responsible for controlling the multifunctional converter and the other for the grid-feeding converter, as shown in Fig. 9. An Agilent DSO-X 2014A oscilloscope, connected to the Typhoon HIL analog outputs is used to capture the results.

The following results evaluate the steady state operation and dynamic responses of the proposed converter under many conditions, such as: grid-feeding operation, controlling active power; series grid-support operation, eliminating voltage disturbances; shunt grid-support operation, reducing current disturbances; stand-alone operation, supplying the microgrid loads; and finally, the grid-connected to islanded transitions of the microgrid.

#### 4.1. Grid-feeding operation

Fig. 10 analyzes the multifunctional converter controlling active power exchanged with the grid, i.e., grid-feeding operation. In this scenario, the grid-feeding converter (GFEC, see in Fig. 9) is disabled. Initially, the power grid fully supplies the linear load with a power

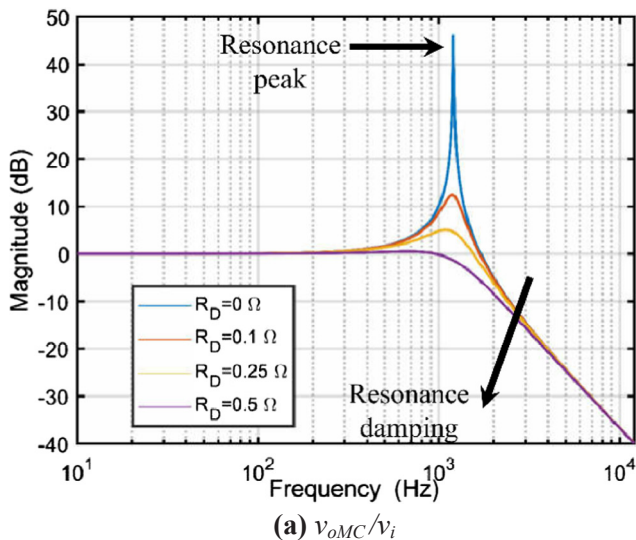
factor equal to 0.8 (lagging), as shown in Table 2. At approximately 120 ms, the multifunctional converter injects 10 kW to supply load active power. In this condition, the grid supplies all the load reactive power. At instant 180 ms, the multifunctional converter generation increases to 25 kW, the nonlinear load is connected to the microgrid and the linear load is turned off. During this new set point, the proposed converter supplies all active power of the load and the grid absorbs the excess energy.

#### 4.2. Grid-supporting operation

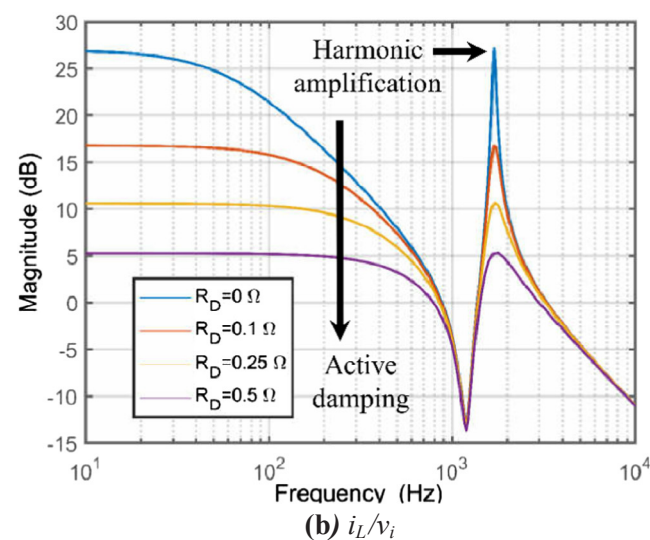
In this scenario, the multifunctional converter operates as a grid-supporting converter and provides ancillary services inherit of series and shunt topologies. The GFEC remains disconnected to the microgrid in this section.

##### 4.2.1. Series connection

When the multifunctional converter operates in series with the microgrid, it is controlled as a voltage source (i.e., mode III) and can act directly in the voltage waveform. Fig. 11 evaluates the multifunctional converter operating as a voltage regulator and series active power filter.



**Fig. 8.** LC filter with active damping: (a)  $v_{oMC}/v_i$ ; (b)  $i_L/v_i$ .



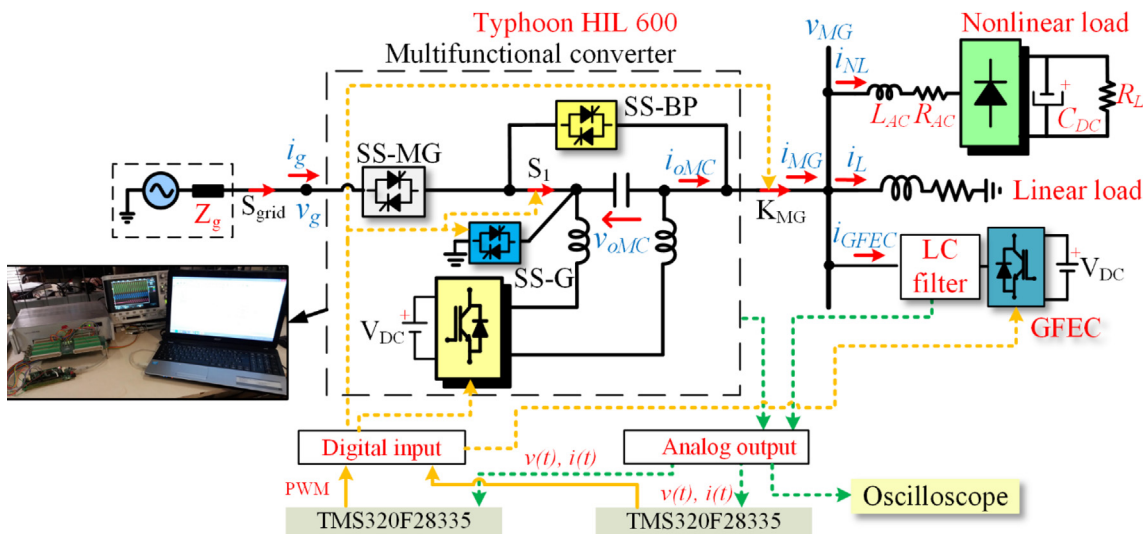


Fig. 9. Hardware-in-the-loop validation.

**Table 2**  
Main electrical parameters of the microgrid system.

| System                        | Parameters   |
|-------------------------------|--|
| Power grid                    | 1Φ, 127 V (1 pu), 60 Hz, $S_{cc} = 1 \text{ MVA}$ , $X/R = 0.5$  |
| Multifunctional converter     | 1Φ VSI, 25 kVA, $f_{sw} = 12 \text{ kHz}$ , $L_1 = 29 \mu\text{H}$ , $R_1 = 11 \text{ m}\Omega$ , $C_f = 308 \mu\text{F}$ , $V_{DC} = 311 \text{ V}$                               |
| Grid-feeding converter (GFEC) | 1Φ VSI, 25 kVA, $f_{sw} = 12 \text{ kHz}$ , $L_1 = 170 \mu\text{H}$ , $R_1 = 64 \text{ m}\Omega$ , $R_f = 50 \text{ m}\Omega$ , $C_f = 100 \mu\text{F}$ , $V_{DC} = 311 \text{ V}$ |
| Linear load                   | 13 kVA, $\text{pf} = 0.8$ lagged   |
| Nonlinear load                | 10 kW, $C_{DC} = 30 \text{ mF}$ , $R_L = 3 \Omega$ , $R_{AC} = 64 \text{ m}\Omega$ , $L_{AC} = 30 \mu\text{H}$   |

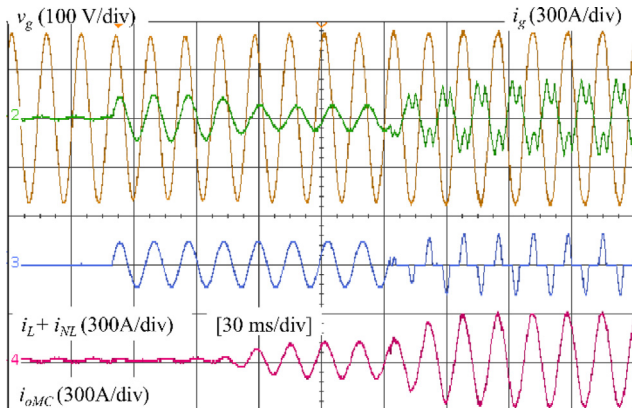


Fig. 10. Grid-feeding operation.

Initially, the grid voltage ( $v_g$ ) is sinusoidal and the nonlinear load is connected to the microgrid. In this condition, the converter compensates the harmonic voltage drop across the grid impedance caused by the distorted current drained by loads. In steady state, the microgrid operates with voltage total harmonic distortion (THD $v_{MG}$ ) equal to 2.3%, and current THD $i_{MG}$  equal to 86% with the nonlinear load. In approximately 120 ms, the grid voltage is intentionally distorted with the following harmonics:  $v_{3h} = 0.1 \text{ pu}$ ,  $v_{5h} = 0.05 \text{ pu}$ ,  $v_{7h} = 0.025 \text{ pu}$ ,  $v_{11h} = 0.01 \text{ pu}$ , and the multifunctional converter acts as a series active filter promptly compensating the voltage disturbances. In steady state, grid voltage waveform is distorted (THD $v_g = 13.13\%$ ), while the microgrid voltage remains practically sinusoidal with THD $v_{MG}$  equal to 2.3% and current THD $i_{MG}$  equal to 86%.

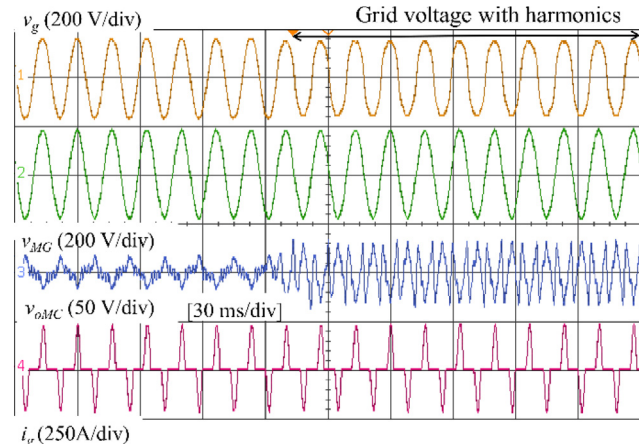


Fig. 11. Series active power filter operation.

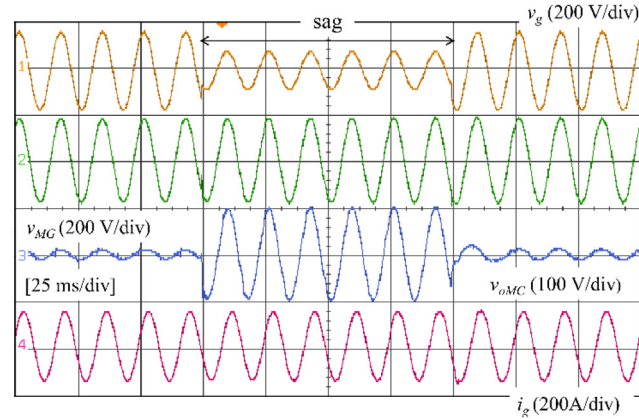


Fig. 12. Sag compensation.

In this configuration, the multifunctional converter can also compensate voltage sags and swells, as shown in Fig. 12 and Fig. 13, respectively. Fig. 12 shows a sag compensation with a residual voltage of 0.5 p.u. and duration of 100 ms. Fig. 13 illustrates a similar scenario, but with a voltage swell of 1.2 p.u. in the grid voltage. In both cases, before and after the disturbances, the microgrid voltage is regulated to 1 p.u., with a sinusoidal waveform.

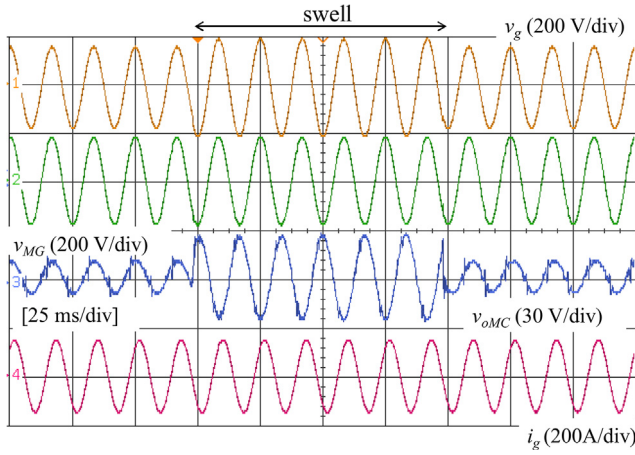


Fig. 13. Swell compensation.

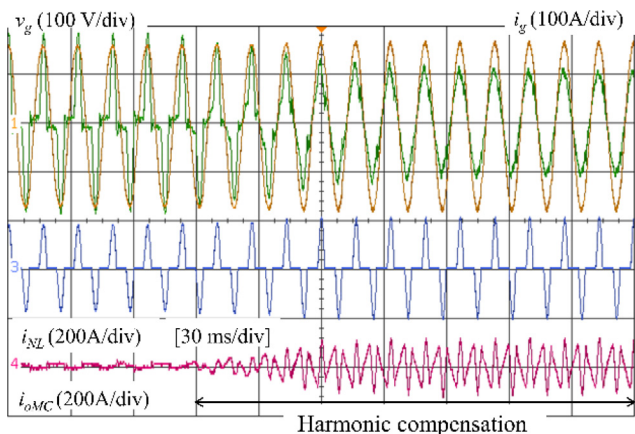


Fig. 14. Shunt active filter compensating harmonics.

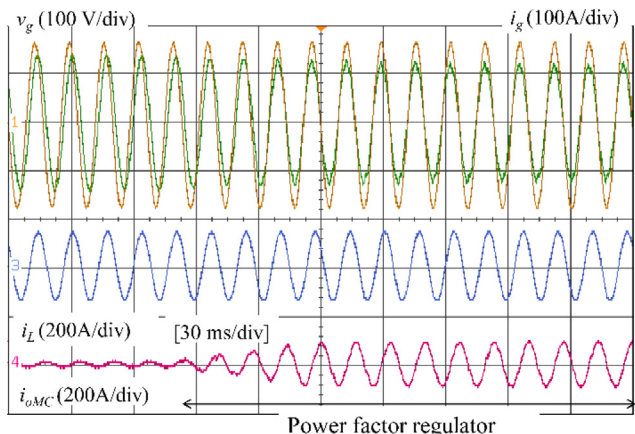


Fig. 15. Shunt active filter improving power factor.

#### 4.2.2. Shunt connection

In the shunt connection scenario, the multifunctional converter is connected in shunt to the microgrid and operates in mode IV. The converter is controlled as a current source and can act directly in the current waveform, as a shunt active power filter. Fig. 14 considers the nonlinear load (harmonic compensation), while Fig. 15 considers the linear load (reactive compensation).

In Fig. 14, the grid current ( $i_g$ ) compensation and its impact on the voltage waveform can be observed that improves due to the reduced crest factor of the current flowing through the line impedance. The grid

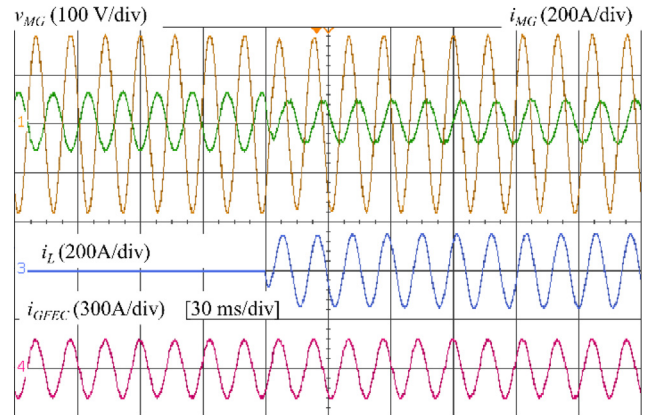


Fig. 16. Stand-alone scenario supplying the linear load.

current THD*i<sub>g</sub>* is reduced from 74.8% to 8.6%. Similarly, the grid voltage THD*v<sub>g</sub>* is decreased from 3.9% to 2.9%. In Fig. 15, the operation as active filter enhances the power factor on the grid side. It can be observed that during power factor regulation, the grid current is in-phase with the voltage, reducing the displacement factor.

#### 4.3. Stand-alone operation

Fig. 16 evaluates the multifunctional converter operating as a grid-forming converter providing stand-alone operation (mode V). Initially, the PCC is supplied by the multifunctional converter, followed sequentially by the loads and the grid-feeding converter. GFEC is connected to the microgrid, and injects 10 kW of active power. At this instant, generated energy is absorbed by the ESS from the multifunctional converter. Then, the linear load is connected at 120 ms, and it is supplied by the power produced by GFEC. The grid-forming converter fully supplies the load reactive power. The multifunctional converter keeps the voltage constant and sinusoidal, with a maximum THD*v<sub>MG</sub>* equal to 1%.

A second scenario is shown in Fig. 17, with the multifunctional converter supplying the nonlinear load. The grid-feeding converter is connected at approximately 130 ms and injects 25 kW into the microgrid. All the load active power is generated by GFEC and the excess power is absorbed by the grid-forming converter. The grid-forming converter fully supplies the harmonics and reactive power of the nonlinear load. The maximum THD*v<sub>MG</sub>* in this scenario is 2.5%.

#### 4.4. Transitions of microgrid operating modes

This section evaluates the transition between microgrid modes of

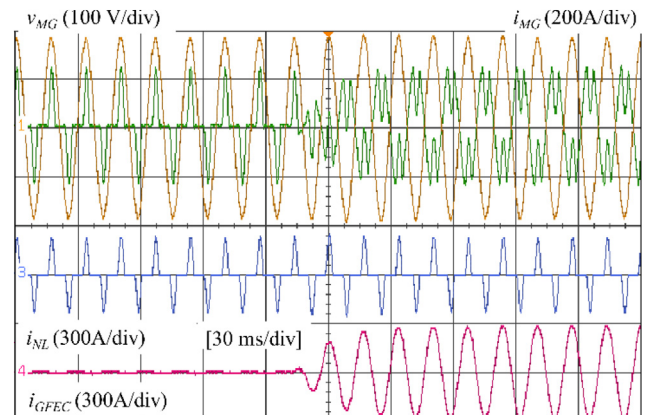
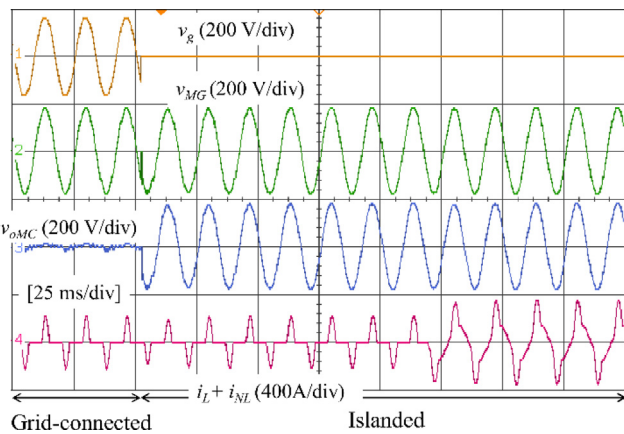


Fig. 17. Stand-alone scenario supplying the nonlinear load.



**Fig. 18.** Transition from series grid-connected to islanded mode.

operation, as shown in Fig. 3. This paper deals only with the intentional islanding.

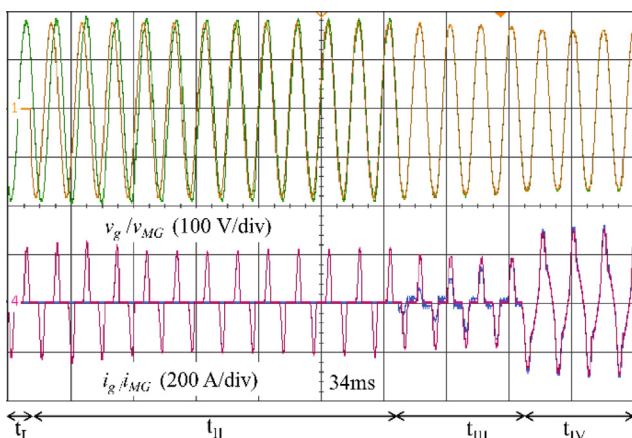
#### 4.4.1. Islanding transition

Fig. 18 shows the islanding transition between modes III to V, i.e., I<sub>T-I</sub>. Initially, the grid supplies the nonlinear load and the multifunctional converter operates as a series device. In approximately 53 ms, the multifunctional converter is smoothly driven to an intentional island and starts running in mode V. Finally, the linear load is connected at time 175 ms. Islanding transition of shunt devices, i.e., I<sub>T-II</sub>, is sufficiently studied in the literature, such as [16,36], and will not be covered herein.

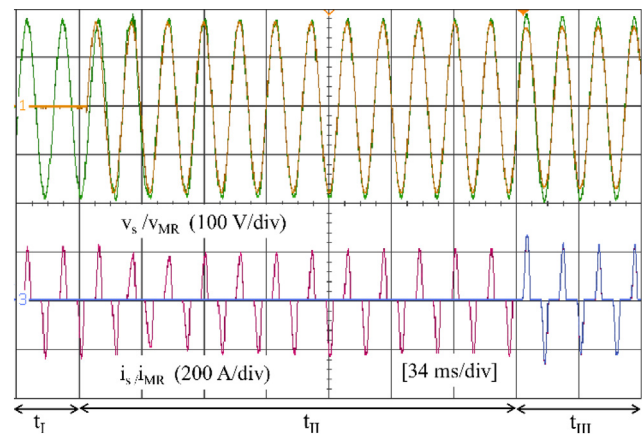
#### 4.4.2. Reconnection transition

Fig. 19 shows the reconnection transition from mode V to mode IV, i.e., R<sub>T-I</sub>. At instant  $t_b$ , the microgrid operates in islanded mode, supplying the nonlinear loads. Once the power grid is restored ( $t_{II}$ ), the multifunctional converter synchronizes with the grid voltage. After synchronization ( $t_{III}$ ), the switches SS-MG and SS-BP are closed (mode IV – shunt connection). The multifunctional converter changes its control to current source and contributes to the microgrid needs. The converter current starts ramping up within four cycles of fundamental frequency. Finally, ( $t_{IV}$ ), the nonlinear load is connected to the microgrid, and the converter operates in standby (i.e., mode II) through transition T<sub>III</sub>.

Fig. 20 shows the reconnection transition from mode V to mode III, i.e., R<sub>T-II</sub>. Initially at instant  $t_b$ , the multifunctional converter provides stand-alone operation. When the power grid is reestablished ( $t_{II}$ ), the microgrid voltage ( $v_{MR}$ ) is synchronized with the grid. At instant  $t_{III}$ ,



**Fig. 19.** Transition from islanded to shunt grid-connected mode.



**Fig. 20.** Transition from islanded to series grid-connected mode.

switches SS-MG and S<sub>1</sub> are closed (mode III – series connection) and the converter operates as a series active filter, completing the reconnection transition.

## 5. Conclusions

This paper presented a multifunctional converter applied to a centralized AC microgrid. The proposed converter can operate in series or parallel connection with the microgrid. It aggregates functionalities from both connection topologies, such as: series active filtering of voltage harmonics, voltage sag and swell compensation, shunt active filtering of current harmonics, power factor correction and voltage regulation through reactive power injection. Moreover, this converter can operate either as voltage- or current-controlled source performing smooth transition between microgrid operating modes, i.e., grid-connected and islanded.

The proposed converter topology is a typical series compensator structure with a single-phase VSI and LC output filter, adding a non-time-critical breaker and two static switches. The control scheme was devised in natural coordinate-frame with active damping to avoid harmonic resonance between the LC filter and power grid. The proposed control of the multifunctional converter was validated through a hardware-in-the-loop simulation implemented in Typhoon HIL 600. The performance of this converter in all steady state modes of operation was evaluated, as well as the most critical transitions R<sub>T-I</sub>, R<sub>T-II</sub>, and I<sub>T-I</sub>, according to Fig. 3. The main results have demonstrated that the multifunctional converter is a promising configuration with a capacity to perform multi-functionalities increasing the cost-benefit of such converters that are required in centralized microgrid architectures, especially those that comprise most susceptible loads and already require series active compensator, such as UPS.

The main contributions of this paper are: (i) a new topology for a multifunctional converter that can operate either as a series or a shunt converter; (ii) a control strategy for the converter that allows its operation as a grid-forming, grid-feeding or a grid-supporting converter; (iii) a control algorithm that allows the seamless transition from the series to the shunt connection and vice-versa.

## Acknowledgements

The authors would like to thank the Graduate Program in Electrical Engineering of the Federal University of Minas Gerais (PPGEE-UFGM) for supporting this research, the government agencies CAPES and CNPQ for their financial support and Typhoon HIL for the technical assistance.

## Appendix A. Supplementary material

Supplementary data associated with this article can be found, in the online version, at <http://dx.doi.org/10.1016/j.ijepes.2018.04.013>.

## References

- [1] Miyagi M, Shiroma Y, Yona A, Senju T, Funabashi T. Uninterruptible smart house equipped with the phase synchronization control system. *Int J Electr Power Energy Syst* 2014;63:302–10. <http://dx.doi.org/10.1016/j.ijepes.2014.05.050>.
- [2] Bouzid AM, Guerrero JM, Cheriti A, Bouhamida M, Sicard P, Benghanem M. A survey on control of electric power distributed generation systems for microgrid applications. *Renew Sustain Energy Rev* 2015;44:751–66. <http://dx.doi.org/10.1016/j.rser.2015.01.016>.
- [3] Li P, Li Y, Yin Z. Realization of UPQC H $\infty$  coordinated control in Microgrid. *Int J Electr Power Energy Syst* 2015;65:443–52. <http://dx.doi.org/10.1016/j.ijepes.2014.10.032>.
- [4] Pecas Lopes JA, Moreira CL, Madureira AG. Defining control strategies for analysing microgrids islanded operation. 2005 IEEE Russia Power Tech, St. Petersburg: IEEE; 2005, p. 1–7. <http://dx.doi.org/10.1109/PTC.2005.4524548>.
- [5] Parhizi S, Lotfi H, Khodaei A, Bahramirad S. State of the art in research on microgrids: a review. *IEEE Access* 2015;3:890–925. <http://dx.doi.org/10.1109/ACCESS.2015.2443119>.
- [6] Hosseiniemehr T, Ghosh A, Shahnia F. Cooperative control of battery energy storage systems in microgrids. *Int J Electr Power Energy Syst* 2017;87:109–20. <http://dx.doi.org/10.1016/j.ijepes.2016.12.003>.
- [7] Rocabert J, Luna A, Blaabjerg F, Rodríguez P. Control of power converters in AC microgrids. *IEEE Trans Power Electron* 2012;27:4734–49. <http://dx.doi.org/10.1109/TPEL.2012.2199334>.
- [8] Majumder R, Bag G. Parallel operation of converter interfaced multiple microgrids. *Int J Electr Power Energy Syst* 2014;55:486–96. <http://dx.doi.org/10.1016/j.ijepes.2013.09.008>.
- [9] Serban I, Ion CP. Microgrid control based on a grid-forming inverter operating as virtual synchronous generator with enhanced dynamic response capability. *Int J Electr Power Energy Syst* 2017;89:94–105. <http://dx.doi.org/10.1016/j.ijepes.2017.01.009>.
- [10] Xu L, Miao Z, Fan L. Coordinated control of a solar and battery system in a microgrid. *PES T&D* 2012, IEEE; 2012, p. 1–7. <http://dx.doi.org/10.1109/TDC.2012.6281700>.
- [11] Azevedo GMS, Cavalcanti MC, Neves FAS, Limongi LR, Bradaschia F. A control of microgrid power converter with smooth transient response during the change of connection mode. In: 2013 Brazilian Power Electronics Conference, IEEE; 2013, p. 285–94. <http://dx.doi.org/10.1109/CBEP.2013.6785238>.
- [12] Zeng Z, Yang H, Zhao R, Cheng C. Topologies and control strategies of multi-functional grid-connected inverters for power quality enhancement: a comprehensive review. *Renew Sustain Energy Rev* 2013;24:223–70. <http://dx.doi.org/10.1016/j.rser.2013.03.033>.
- [13] Teke A, Latran MB. Review of multifunctional inverter topologies and control schemes used in distributed generation systems. *J Power Electron* 2014;14:324–40. <http://dx.doi.org/10.6113/JPE.2014.14.2.324>.
- [14] Bacha S, Picault D, Burger B, Etxeberria-Otadui I, Martins J. Photovoltaics in microgrids: an overview of grid integration and energy management aspects. *IEEE Ind Electron Mag* 2015;9:33–46. <http://dx.doi.org/10.1109/MIE.2014.2366499>.
- [15] Zhang Z, Chen W, Zhang Z. A new seamless transfer control strategy of the microgrid. *The Scientific World J* 2014;2014:1–9. <http://dx.doi.org/10.1155/2014/391945>.
- [16] Tenti P, Caldognetto T, Buso S, Brandão DI. Control of utility interfaces in low-voltage microgrids. *Eletrônica de Potência* 2015;20:373–82. <http://dx.doi.org/10.18618/REP.2015.4.2556>.
- [17] Wang J, Chang NCPNCP, Feng X, Monti A. Design of a generalized control algorithm for parallel inverters for smooth microgrid transition operation. *IEEE Trans Ind Electron* 2015;62:4900–14. <http://dx.doi.org/10.1109/TIE.2015.2404317>.
- [18] Han X, Cheng R, Wang P, Jia Y. Advanced dynamic voltage restorer to improve power quality in microgrid, n.d. <http://dx.doi.org/10.1109/PESMG.2013.6672665>.
- [19] Silva SM, Filho BJC. Component-minimized voltage sag compensators. In: conference record of the 2002 IEEE industry applications conference. 37th IAS annual meeting, vol. 2, IEEE; 2002, p. 883–9. <http://dx.doi.org/10.1109/IAS.2002.1042663>.
- [20] e Silva FSF, de S, Ribeiro LA, de Matos JG. Bidirectional DC-AC converter for isolated microgrids with voltage unbalance reduction capabilities. In: 2014 IEEE Energy Conversion Congress and Exposition (ECCE), IEEE; 2014, p. 4985–91. <http://dx.doi.org/10.1109/ECCE.2014.6954085>.
- [21] Farhad-Kangarlu M, Babaei E, Blaabjerg F. A comprehensive review of dynamic voltage restorers. *Int J Electr Power Energy Syst* 2017;92:136–55. <http://dx.doi.org/10.1016/j.ijepes.2017.04.013>.
- [22] He J, Li YW. Generalized closed-loop control schemes with embedded virtual impedances for voltage source converters with LC or LCL filters. *IEEE Trans Power Electron* 2012;27:1850–61. <http://dx.doi.org/10.1109/TPEL.2011.2168427>.
- [23] Teodorescu R, Liserre M, Rodriguez P. Grid Converters for Photovoltaic and Wind Power Systems. WILEY, Chichester, UK: John Wiley & Sons, Ltd; 2011. <http://dx.doi.org/10.1002/9780470667057>.
- [24] Grilo R, Costa-Castelló R. Digital repetitive plug-in controller for odd-harmonic periodic references and disturbances. *Automatica* 2005;41:153–7. <http://dx.doi.org/10.1016/j.automatica.2004.08.006>.
- [25] Chen S, Lai YM, Tan S-C, Tse CK. Analysis and design of repetitive controller for harmonic elimination in PWM voltage source inverter systems. *IET Power Electron* 2008;1:497. <http://dx.doi.org/10.1049/iet-pel:20070006>.
- [26] Buso S, Mattavelli P. Digital Control in Power Electronics, 2nd ed. Synthesis Lectures on Power Electronics, vol. 5; 2015, p. 1–229. <http://dx.doi.org/10.2200/S00637ED1V01Y201503PEL007>.
- [27] Antunes H, Silva S, Filho B, Ferreira R, Brandao DI. A new configuration for a grid forming converter in AC Islanded microgrid. In: PCIM Europe 2017; International Exhibition and Conference for Power Electronics, Intelligent Motion, Renewable Energy and Energy Management; 2017, p. 1–8.
- [28] Ryan MJ, Brumsickle WE, Lorenz RD. Control topology options for single-phase UPS inverters. *IEEE Trans Ind Appl* 1997;33:493–501. <http://dx.doi.org/10.1109/28.568015>.
- [29] Zhou Keliang, Wang D, Fang-Lin Luo, Bin Zhang, Yigang Wang. Zero-phase odd-harmonic repetitive controller for a single-phase PWM inverter. *IEEE Trans Power Electron* 2006;21:193–201. <http://dx.doi.org/10.1109/TPEL.2005.861190>.
- [30] Yazdani A, Iravani R. Voltage-sourced converters in power systems: modeling, control, and applications. Hoboken, NJ, USA: John Wiley & Sons, Inc.; 2010.
- [31] Pádua MS, Deckmann SM, Sperandio GS, Marafão FP, Colón D. Comparative analysis of synchronization algorithms based on PLL, RDFT and Kalman Filter. *IEEE Int Symp Ind Electron* 2007:964–70. <http://dx.doi.org/10.1109/ISIE.2007.4374728>.
- [32] Guo W, Mu L. Control principles of micro-source inverters used in microgrid. *Protect Control Modern Power Syst* 2016;1:5. <http://dx.doi.org/10.1186/s41601-016-0019-8>.
- [33] Paredes HKM, Marafão FP, Brandão DI, Costabeber A. Multi-task control strategy for grid-tied inverters based on conservative power theory. *IET Renew Power Gener* 2015;9:154–65. <http://dx.doi.org/10.1049/iet-rpg.2014.0065>.
- [34] Blasko V, Kaura V. A novel control to actively damp resonance in input LC filter of a three-phase voltage source converter. *IEEE Trans Ind Appl* 1997;33:542–50. <http://dx.doi.org/10.1109/28.568021>.
- [35] Kim H-S, Sul S-K. A novel filter design for output LC filters of PWM inverters. *J Power Electron* 2011;11:74–81. <http://dx.doi.org/10.6113/JPE.2011.11.1.074>.
- [36] Kwon J, Yoon S, Choi S, Member S. Indirect current control for seamless transfer of three-phase utility interactive inverters. *IEEE Trans Power Electron* 2012;27:773–81. <http://dx.doi.org/10.1109/TPEL.2011.2161335>.